

Kondo physics of reconstructed vacancies in graphene

Andrew K. Mitchell^{1,2} and Lars Fritz¹

¹*Institut für Theoretische Physik, Universität zu Köln, Zùlpicher Straße 77, 50937 Köln, Germany*

²*Department of Chemistry, Physical and Theoretical Chemistry,
Oxford University, South Parks Road, Oxford OX1 3QZ, United Kingdom*

(Dated: December 13, 2012)

Defects in the honeycomb lattice of graphene are known to induce local moments and strong correlation effects. Distortions due to structural reconstruction around vacancies in graphene were studied recently by Cazalilla *et al.* [[arXiv:1207.3135 \(2012\)](#)], who formulated an effective model consisting of a localized σ level hybridized with the π -band. We analyze the rich quantum impurity physics of this system using a combination of numerical renormalization group and analytical techniques, focusing on the special role played by the unusual local density of states, which is enhanced at low energies due to potential scattering. Depending on microscopic parameters, the model hosts both exactly-screened spin-1/2 (doublet) Kondo or underscreened spin-1 (triplet) Kondo phases, and we study the quantum phase transition separating them. Although the effective Kondo models also support new stable phases characterized by strong renormalized particle-hole asymmetry, such phases cannot in fact be accessed in the full Andersonian model describing the vacancy. We show that distinctive signatures of the modified powerlaw Kondo effect thus always appear at low energies in thermodynamic quantities and the scattering t matrix.

PACS numbers: 73.22.Pr, 72.15.Qm, 72.10.Fk

Since its experimental isolation, graphene has attracted a great deal of attention on both experimental and theoretical fronts alike.^{1–3} Remarkably, most of the novel properties of graphene can be explained within a simple non-interacting single particle picture. However, richer physics naturally results when strong electron correlations and formation of magnetic moments play a key role, as is the case for example when transition metal atoms are adsorbed onto the graphene surface.

In standard metals, the Kondo effect describes screening of such local moments by quantum many-body spin-singlet formation at low temperatures,⁴ which constitutes a classic paradigm of strong correlations in condensed matter science. But due to the peculiar nature of the low-energy degrees of freedom in bulk graphene,^{5–10} including the vanishing density of states at the Dirac point, magnetic impurities may exhibit unusual Kondo physics, and even local quantum phase transitions.^{10–14}

Defects in graphene, such as carbon vacancies and induced reconstructions in the otherwise perfect honeycomb lattice, can also give rise to interesting new physics.^{15–19} In particular, evidence of the Kondo effect has been observed experimentally in irradiated graphene samples which host such vacancies.^{20–22} It was argued recently by Cazalilla *et al.* in Ref. 19 that structural corrugations around vacancies allow for a hybridization between the σ - and π -orbitals, which leads to local magnetic moment formation (an effect absent in flat graphene). Potential scattering from the defect induces a greatly enhanced density of conduction electron states coupling to these local moments.¹⁹ This can potentially give rise to very high Kondo temperatures, as observed already in certain experiments.²² For a thorough recent review of Kondo physics in graphene, see Ref. 23.

In this paper we study in detail the effective model for

isolated vacancies in graphene given in Ref. 19. The very unusual local density of states leads to a variant of the pseudogap Kondo problem, giving rise to exotic quantum impurity physics. For example, the residual impurity entropy of $S_{\text{imp}} = -k_B \ln(4)$ is the lowest possible for this type of system. The complex orbital structure of the underlying impurity problem also supports a quantum phase transition separating doublet and underscreened triplet Kondo phases. We go beyond the previous perturbative analysis, using the full numerical renormalization group (NRG) to calculate various physical quantities exactly (for a recent review of the technique, see Ref. 24). Numerical results are supported wherever possible by analytical arguments.

Our main results are as follows:

- (i) Phase diagrams for the effective Kondo models with spin $S = 1/2$ (doublet) and $S = 1$ (triplet) are presented and discussed. In both cases, the modified powerlaw density of states supports two distinct strong coupling phases, corresponding to runaway RG flow of either the Kondo exchange coupling or potential scattering. Thermodynamic and dynamical quantities are analyzed analytically at the various stable fixed points, while the full crossover between fixed points is calculated numerically. The quantum critical physics associated with the phase transition separating strong coupling states is studied for both doublet and triplet Kondo models.
- (ii) The quantum phase transition between $S = 1/2$ and $S = 1$ Kondo screened phases of the full Andersonian model is analyzed. We find that the quantum phase transition is a simple level crossing.
- (iii) We find that the particle-hole asymmetric local moment phases of the simplified Kondo models are *not* accessible in the underlying full Andersonian model, and hence will not in practice be realized in experiments.

The organization of the manuscript is as follows: Following Ref. 19, we introduce the coupled two-impurity Anderson model describing the reconstructed graphene vacancy in Sec. I. Depending on the strength of the Hund's rule coupling, both $S = 1/2$ and $S = 1$ 'impurity' configurations can be realized. Deep in either regime, effective low-energy Kondo models can be derived, which are studied explicitly in Sec. II. Thermodynamic and dynamical quantities are calculated in each phase of each model, and their phase diagrams are analyzed in detail. Physical behavior in the vicinity of the stable strong coupling fixed points is understood and interpreted in terms of a resonant level or pure potential scatterer. The evolution of strong coupling scales is extracted in each case. We also examine the quantum phase transition separating Kondo screened and asymmetric local moment states in the doublet and triplet Kondo models.

In Sec. III we analyze the full Andersonian model, and argue that certain phases of the Kondo model are not in fact accessible. However, a level-crossing quantum phase transition separating doublet and triplet Kondo screened phases is accessible, and we study it in detail. We conclude with a discussion of our results in Sec. IV. More technical parts of the analysis are relegated to the appendix.

I. MODEL AND OBSERVABLES

The underlying Anderson model for a single vacancy in graphene was presented in Ref. 19. It is formulated in terms of two hybridized local quantum orbitals of the σ and π bands, denoted d_σ and π_σ respectively. The spin density of these orbitals, $\mathbf{S}_d = \frac{1}{2}d_\sigma^\dagger \vec{\sigma}_{\sigma\sigma'} d_{\sigma'}$ and $\mathbf{S}_\pi = \frac{1}{2}\pi_\sigma^\dagger \vec{\sigma}_{\sigma\sigma'} \pi_{\sigma'}$, interact via the Hund's rule coupling J_H . Local electron correlations on the d -level, parametrized by U , and a capacitive interaction $U_{\sigma\pi}$ acting between d and π levels are also important.¹⁹ We allow for tunneling of electrons between the levels as well as the hybridization of the d -level with the conduction electrons of the graphene host. The full Hamiltonian is $H = H_0 + H_{\text{imp}} + H_{\text{hyb}}$, where

$$\begin{aligned} H_0 &= \sum_{\mathbf{k},\sigma} \epsilon_{\mathbf{k}} c_{\mathbf{k},\sigma}^\dagger c_{\mathbf{k},\sigma} , \\ H_{\text{imp}} &= \epsilon_d n_d + U n_d^\uparrow n_d^\downarrow + \epsilon_\pi n_\pi + U_{\sigma\pi} n_d n_\pi \\ &\quad - J_H \mathbf{S}_d \cdot \mathbf{S}_\pi + g \sum_{\sigma} (d_\sigma^\dagger \pi_\sigma + \text{H.c.}) , \\ H_{\text{hyb}} &= v_{\text{hyb}} \sum_{\mathbf{k},\sigma} \left(c_{\mathbf{k},\sigma}^\dagger d_\sigma + \text{H.c.} \right) . \end{aligned} \quad (1)$$

Here, $c_{\mathbf{k},\sigma}$ denotes the conduction electrons, and $n_d = \sum_{\sigma} n_d^\sigma = \sum_{\sigma} d_\sigma^\dagger d_\sigma$ is the total number operator for the d -level, while for the π -level, $n_\pi = \sum_{\sigma} n_\pi^\sigma = \sum_{\sigma} \pi_\sigma^\dagger \pi_\sigma$.

Importantly, the local conduction electron density at the defect site, $\rho(\omega) \propto \sum_{\mathbf{k}} \delta(\omega - \epsilon_{\mathbf{k}})$, is strongly modified

by potential scattering.¹⁹ It assumes the diverging but normalizable form

$$\rho(\omega) = \frac{1}{2} \frac{\ln(\Lambda/D_0)}{|\omega| \ln^2 |\omega/\Lambda|} \theta(D_0 - |\omega|) , \quad (2)$$

where D_0 is a high-energy cutoff for the conduction band (the precise choice of which is irrelevant for the low-energy quantum impurity physics). We stress that the second cutoff $\Lambda > D_0$ is necessary for the density of states to be normalizable. In a real system, Λ corresponds physically to the scale above which the density of states is not well-described by Eq. (2) because high-energy details of the graphene band structure become important. In particular, we note that the Kondo temperature T_K will thus naturally depend on the couplings and also on Λ .

The retarded free local electronic Green function at the defect site follows from the local density of states, Eq. (2), as

$$\begin{aligned} G_{\text{loc}}^{(0)}(\omega) &= \mathcal{P} \int d\epsilon \frac{\rho(\epsilon)}{\omega - \epsilon} - i\pi\rho(\omega) , \\ &\stackrel{\omega \rightarrow 0}{=} -\frac{\pi \ln \frac{\Lambda}{D_0}}{2|\omega| \ln^2 |\frac{\omega}{\Lambda}|} \left(\frac{2}{\pi} \ln \left| \frac{\omega}{\Lambda} \right| \text{sgn}(\omega) + i \right) , \end{aligned} \quad (3)$$

where \mathcal{P} denotes the principal value, and the second line is obtained analytically at low frequencies, as sketched in Appendix A.

The hybridization function for the d -level, $\Delta(\omega) = v_{\text{hyb}}^2 G_{\text{loc}}^{(0)}(\omega)$, contains all the information about the non-interacting bath of conduction electrons and, together with H_{imp} , completely specifies the underlying quantum impurity problem. As demonstrated in the following, the model can then be solved numerically exactly within NRG by exploiting a logarithmic discretization of this hybridization function.

For realistic model parameters,²⁵ there are two relevant regimes of the isolated d - π level system described by H_{imp} . The parameter $G = \frac{J_H}{4U_{\sigma\pi}}$ essentially controls the occupancy of the π -level. For $G \ll 1$, the π -level is essentially empty, $\langle n_\pi \rangle \simeq 0$; while for $G \gg 1$, the π -level is singly-occupied, $\langle n_\pi \rangle \simeq 1$. When the d -level is also singly-occupied (as obtained for $-U \ll \epsilon_d \ll 0$), the ground state of H_{imp} is thus a doublet for $G \ll 1$, but a triplet when $G \gg 1$ by virtue of the ferromagnetic Hund's coupling.

A. Effective low-energy Kondo models

On hybridization with the graphene conduction electrons, low-energy effective Kondo models can be derived using the standard Schrieffer-Wolff transformation,⁴ provided $v_{\text{hyb}}^2/U \ll 1$. Projecting onto the doublet or triplet manifolds of H_{imp} by perturbatively eliminating virtual

charge fluctuations to second order in v_{hyb} , one obtains

$$H_K = H_0 + J_K \mathbf{S} \cdot \mathbf{s}_0 + V \sum_{\mathbf{k}, \mathbf{k}', \sigma} c_{\mathbf{k}, \sigma}^\dagger c_{\mathbf{k}', \sigma} \quad (4)$$

where $\mathbf{S} = \mathbf{S}_d + \mathbf{S}_\pi$ is the total spin of the d - π subsystem; and $\mathbf{s}_0 = \frac{1}{2} \sum_{\mathbf{k}, \mathbf{k}'} c_{\mathbf{k}, \sigma}^\dagger \vec{\sigma}_{\sigma\sigma'} c_{\mathbf{k}', \sigma'}$. In the doublet regime we thus have an $S = 1/2$ Kondo model, while in the triplet regime an $S = 1$ Kondo model results. Since Kondo models with different impurity spin give different ground states,⁴ the low-energy mapping of the full model Eq. (1) onto the effective Kondo models Eq. (4) imply the existence of a quantum phase transition on tuning G . This scenario is explored in detail in Sec. III B. The effective parameters of these Kondo models are given by,

$$\begin{aligned} J_K &\simeq 2|v_{\text{hyb}}|^2 \left[\frac{1}{|\tilde{\epsilon}_d|} + \frac{1}{|U + \tilde{\epsilon}_d|} \right] \\ V &\simeq \frac{|v_{\text{hyb}}|^2}{2} \left[\frac{1}{|\tilde{\epsilon}_d|} - \frac{1}{|U + \tilde{\epsilon}_d|} \right] \end{aligned} \quad (5)$$

where $\tilde{\epsilon}_d = \epsilon_d$ in the doublet case, while in the triplet case $\tilde{\epsilon}_d = \epsilon_d + U_{\sigma\pi} - J_H/4$. It is important to note that in both cases the Kondo coupling $J_K > 0$ is antiferromagnetic. Of course, the novel feature of these Kondo models is the unusual density of states, Eq. (2), whose modified powerlaw behavior is shown to result in rich quantum impurity physics.

B. Physical observables

In the following, we consider thermodynamic properties of the above Andersonian and Kondo models. In particular, we wish to calculate impurity contributions to the entropy, $S_{\text{imp}}(T)$, and the magnetic susceptibility $\chi_{\text{imp}}(T) = \langle (\hat{S}_{\text{tot}}^z)^2 \rangle_{\text{imp}} / T$, as a function of temperature, T . As usual,⁴ $\langle \hat{\Omega} \rangle_{\text{imp}} = \langle \hat{\Omega} \rangle - \langle \hat{\Omega} \rangle_0$, with $\langle \hat{\Omega} \rangle_0$ denoting the thermal average for the free system. The behavior of these quantities allows straightforward identification of the various fixed points, and evince clear RG flow. Crossovers between these fixed points also provides direct access to the underlying energy scales of the problem, such as the Kondo temperature, T_K .

In addition, we study dynamic quantities, focusing on the energy-dependence of the t matrix. Since the t matrix controls the scanning tunneling spectroscopic response and resistivity measurements, it is the key quantity needed to interpret certain experimental results. The rapid and universal evolution of the t matrix at energies on the order of the Kondo temperature could thus provide the ‘smoking gun’ signature of Kondo physics in a graphene system with isolated vacancies.

The t matrix describes scattering between diagonal states \mathbf{k} and \mathbf{k}' of H_0 induced by the defect. It is generically given by,

$$\begin{aligned} G_{\mathbf{k}, \mathbf{k}'}(\omega) &= G_{\mathbf{k}, \mathbf{k}}^{(0)}(\omega) \delta_{\mathbf{k}\mathbf{k}'} \\ &+ G_{\mathbf{k}, \mathbf{k}}^{(0)}(\omega) \mathcal{T}_{\mathbf{k}, \mathbf{k}'}(\omega) G_{\mathbf{k}', \mathbf{k}'}^{(0)}(\omega), \end{aligned} \quad (6)$$

where $\mathcal{T}_{\mathbf{k}, \mathbf{k}'}(\omega)$ are components of the t matrix. Since hybridization between the d -level and the host is local in space, one readily obtains,

$$G_{\text{loc}}(\omega) = G_{\text{loc}}^{(0)}(\omega) + \left[G_{\text{loc}}^{(0)}(\omega) \right]^2 T(\omega), \quad (7)$$

where $T(\omega) = N \mathcal{T}_{\mathbf{k}, \mathbf{k}'}(\omega)$ and $N \rightarrow \infty$ is the number of graphene conduction orbitals.

For the full Anderson model, Eq. (1) the t matrix follows as

$$\mathcal{T}_{\mathbf{k}, \mathbf{k}'}(\omega) = v_{\text{hyb}}^2 G_{dd}(\omega), \quad (8)$$

where $G_{dd}(\omega) \equiv \langle \langle d_\sigma; d_\sigma^\dagger \rangle \rangle_\omega$ is the d -level Green function.

At low energies in the Kondo regime, the same scattering should be produced by the corresponding Kondo models, Eq. (4). The t matrix is then expressed as,

$$\mathcal{T}_{\mathbf{k}, \mathbf{k}'}(\omega) = \mathcal{T}_{\mathbf{k}, \mathbf{k}'}^{ps}(\omega) + \mathcal{T}_{\mathbf{k}, \mathbf{k}'}^K(\omega), \quad (9)$$

where

$$\mathcal{T}_{\mathbf{k}, \mathbf{k}'}^{ps}(\omega) = \left(\frac{V}{1 - V G_{\text{loc}}^{(0)}(\omega)} \right) \quad (10a)$$

$$\mathcal{T}_{\mathbf{k}, \mathbf{k}'}^K(\omega) = \left(\frac{J_K/2}{1 - V G_{\text{loc}}^{(0)}(\omega)} \right)^2 \langle \langle \hat{\gamma}; \hat{\gamma}^\dagger \rangle \rangle_\omega, \quad (10b)$$

with $\hat{\gamma} = \hat{S}^z c_{0, \uparrow} + \hat{S}^- c_{0, \downarrow}$ (here $c_{0, \sigma} = \frac{1}{\sqrt{N}} \sum_{\mathbf{k}} c_{\mathbf{k}, \sigma}$ is a local operator for the conduction electrons at the defect site and \hat{S}^z, \hat{S}^- denote operators for the impurity spin). $\mathcal{T}_{\mathbf{k}, \mathbf{k}'}^{ps}(\omega)$ is the trivial contribution to scattering from a local potential, while $\mathcal{T}_{\mathbf{k}, \mathbf{k}'}^K(\omega)$ describes the effect on scattering due to electron correlations, such as the Kondo effect. Below, we consider explicitly the spectrum of the t matrix, *i.e.*,

$$t(\omega) = -\frac{1}{\pi} \text{Im } T(\omega) \equiv -\frac{1}{\pi} N \text{Im } \mathcal{T}_{\mathbf{k}, \mathbf{k}'} . \quad (11)$$

II. KONDO MODELS

As discussed above, when charge fluctuations are frozen out on the d - and π -levels, the low-energy physics of the reconstructed vacancy is described by a Kondo model, with either an effective $S = 1/2$ or $S = 1$ local moment coupled to the graphene conduction electrons. These models are a close relative of the pseudogap Kondo problem,^{11–14, 26–30} where the density of states is given generically by $\rho(\omega) \propto |\omega|^r$. Such models have been studied extensively, especially for $S = 1/2$ in the context of certain high- T_c superconductors and magnetic impurities in regular graphene,¹⁰ which both realize the $r = 1$ case. Vojta and Bulla considered the case $-1 < r < 0$, describing a spin-1/2 impurity coupled to a diverging density of states.³¹ Although their survey allowed to identify the topology of the phase diagram, details of the various

crossovers and properties of the fixed points themselves were not established exactly. Further detailed study of the generalized powerlaw Kondo model for arbitrary antiferromagnetic or ferromagnetic Kondo coupling will be considered in a separate publication.³²

A. Analytical results

1. Generalized poor man's scaling

Before solving the model numerically exactly using NRG, we first consider perturbative scaling for the $S = 1/2$ and $S = 1$ Kondo models, Eq. (4), with density of states given by Eq. (2). A similar analysis was performed in Ref. 19 for a Kondo model with a related density of states, although the role of the cutoff Λ was not appreciated.

We demonstrate below that two scaling invariants arise for both $S = 1/2$ and $S = 1$ models, corresponding to RG flow of the Kondo coupling J_K and potential scattering V . Strong coupling scales T_K and T_P can thus be estimated, and are shown to depend on Λ as well as the bare couplings and the band cutoff D_0 .

In the spirit of Anderson's poor man's scaling^{19,31,33} we derive flow equations in terms of the dimensionless couplings $j = \frac{J_K}{D \ln^2 \frac{D}{\Lambda}} \ln \frac{\Lambda}{D_0}$ and $v = \frac{V}{D \ln^2 \frac{D}{\Lambda}} \ln \frac{\Lambda}{D_0}$, viz:

$$\begin{aligned} \frac{dj}{d \ln D} &= \left(-1 - \frac{2}{\ln \frac{D}{\Lambda}} \right) j - j^2 + \mathcal{O}(j^3), \\ \frac{dv}{d \ln D} &= \left(-1 - \frac{2}{\ln \frac{D}{\Lambda}} \right) v. \end{aligned} \quad (12)$$

Remarkably, the second equation describing scaling of the potential scattering term is exact to all orders. The coefficient of the linear terms is the scaling dimension and here it depends upon the running scale D and the bare 'cutoff' Λ . Both scaling equations can be solved analytically to yield the scale dependent couplings:

$$\begin{aligned} j(D) &= \frac{\rho(D)}{\rho(D_0)} \frac{j(D_0)}{1 + \frac{j(D_0)}{\rho(D_0)} \int_{D_0}^D \frac{\rho(D')}{D'} dD'}, \\ v(D) &= \frac{\rho(D)}{\rho(D_0)} v(D_0). \end{aligned} \quad (13)$$

An immediate observation is that the strong coupling phases vanish as $\Lambda \rightarrow D_0^+$ since then $j(D), v(D) \rightarrow 0$. The density of states, Eq. (2), reduces to a pair of poles at $\pm D_0$ in this limit, and so there are no low-energy bath degrees of freedom to which the impurity spin can couple. However, in the generic case $\Lambda > D_0$, the running Kondo coupling $j(D)$ and potential scattering $v(D)$ are renormalized upward on successive reduction of the bandwidth/energy scale. The strong coupling scales T_K and T_P associated with the divergence can be identified approximately as the point where these couplings become

of order unity: *i.e.* $j(T_K) = 1$ and $v(T_P) = 1$. Of course, such a perturbative approach breaks down before this point, but such an analysis does provide a useful analytic estimate.

To leading order, it suffices to consider the scaling dimension of the flow equations. To this level of approximation, the flow of j and v is identical, and so the resulting strong coupling scales have the same functional dependence,

$$\begin{aligned} T_K \ln^2 \frac{T_K}{\Lambda} &= \frac{J_K}{2} \ln \frac{\Lambda}{D_0}, \\ T_P \ln^2 \frac{T_P}{\Lambda} &= \frac{V}{2} \ln \frac{\Lambda}{D_0}. \end{aligned} \quad (14)$$

In the limit of small J_K (V), and consequently small T_K (T_P), Eq. (14) can be inverted to yield

$$\begin{aligned} T_K &\approx \frac{J_K}{2} \frac{\ln \frac{\Lambda}{D_0}}{\ln^2 \frac{J_K}{\Lambda}}, \\ T_P &\approx \frac{V}{2} \frac{\ln \frac{\Lambda}{D_0}}{\ln^2 \frac{V}{\Lambda}}. \end{aligned} \quad (15)$$

The notable feature here is that the strong coupling scales are proportional to the bare couplings J_K and V . Of course, this is in marked contrast to the standard metallic case, where $\rho(\omega) \equiv \rho_0$ is finite and constant at low energies. An exponentially small Kondo temperature,⁴ $T_K \propto \exp(-1/\rho_0 J_K)$, results in that case. Remarkably, strong coupling physics in the defective graphene system should be expected at relatively high temperatures.¹⁹

Below, we extract the exact dependence of T_P on V in the pure potential scattering case ($J_K = 0$). In Sec. II C we go further and extract T_K and T_P from exact non-perturbative NRG calculations for the non-trivial case where $V \neq 0$ and $J_K \neq 0$.

The implication from the RG scaling equations, Eq. (13), is that at high energies the physics is controlled by a 'local moment' (LM) fixed point, describing a free impurity spin, decoupled from the bare host (the impurity spin is either $S = 1/2$ or $S = 1$, as above). For larger bare J_K ($\gg V$), the Kondo coupling is renormalized faster as the temperature/energy scale is reduced, and hence the Kondo effect will dominate. For $S = 1/2$, the ground state is then described by a 'symmetric strong coupling' (SSC) fixed point, and the impurity spin is screened by conduction electrons. The remaining Fermi liquid host degrees of freedom now also feel an additional phase shift (equivalent to a modified boundary condition at the defect site) due to the Kondo effect. In the present case of a diverging free density of states, this results in an additional anomalous host contribution to physical properties, as shown below. For impurity spin $S = 1$ the impurity is in fact *underscreened*,^{4,19} and the fixed point is denoted 'USSC'. Alternatively, if the potential scattering is initially very strong ($V \gg J_K$), then V is renormalized faster and the ground state is described by the 'asymmetric local moment' (ALM) fixed point. Although

the impurity (either spin $S = 1/2$ or $S = 1$) remains free, the renormalized potential scattering in the host becomes maximal and similarly generates an anomalous contribution to physical properties. A critical point, (U)AF-CR, separates the (U)SSC and ALM phases. The topology of the flow diagram is shown in Fig. 1, and explicitly discussed in Sec. II B where the physical picture is confirmed by means of exact numerics. The underlying topology of the phase diagram is thus equivalent to that studied in the pure powerlaw case by Vojta and Bulla.³¹

2. Potential scatterer

The simplest limit of the Kondo model arises for $J_K = 0$ in Eq. (4). The model is then trivial in the sense that it is non-interacting, and Kondo physics *per se* is totally absent. However, as suggested by the flow equation, Eq. (13), this simple system has a strong coupling ground state, characterized by potential scattering whose strength diverges below an emergent scale, T_P . Later, it will be shown that the low-energy behavior of the Kondo model with $J_K > 0$ can also be understood in terms of the pure potential scatterer throughout the ALM phases. We discuss briefly this limit now.

The local Green function at the defect site is modified due to the additional potential scattering for $V \neq 0$. It is expressed exactly as,

$$[G_{\text{loc}}(\omega)]^{-1} = [G_{\text{loc}}^{(0)}(\omega)]^{-1} - V. \quad (16)$$

Rearranging this equation in the form of Eq. (7) immediately yields the t matrix for the pure potential scatterer, Eq. (10a). The corresponding spectrum has the following asymptotic forms,

$$t(\omega) \stackrel{|\omega| \ll |V|}{\approx} \left(\frac{1}{2 \ln \frac{\Lambda}{D_0}} \right) |\omega| - \left(\frac{\text{sgn}[\omega]}{V \ln^2 \frac{\Lambda}{D_0}} \right) |\omega|^2 \ln \left| \frac{\omega}{\Lambda} \right| + \mathcal{O}(|\omega|^3), \quad (17a)$$

$$\stackrel{|\omega| \gg |V|}{\approx} \frac{1}{2} V^2 \ln \frac{\Lambda}{D_0} \left(\frac{1}{|\omega| \ln^2 |\omega/\Lambda|} \right) + \mathcal{O}(1/|\omega|^2). \quad (17b)$$

By demanding $\partial t(\omega)/\partial \omega = 0$, we find that the spectral peak for small V arises when,

$$V_P = -\omega_P \ln \left| \frac{\omega_P}{\Lambda} \right| / \ln \frac{\Lambda}{D_0}. \quad (18)$$

As $\omega_P \rightarrow 0$, the spectrum exhibits scaling in terms of ω/ω_P , viz:

$$\frac{t(\omega)}{|\omega|} \stackrel{|\omega| \ll |\omega_P|}{\approx} \left(\frac{1}{2 \ln \frac{\Lambda}{D_0}} \right) + \left(\frac{\text{sgn}[\omega V]}{\ln \frac{\Lambda}{D_0}} \right) \left| \frac{\omega}{\omega_P} \right| + \mathcal{O}(|\omega/\omega_P|^2), \quad (19a)$$

$$\stackrel{|\omega| \gg |\omega_P|}{\approx} \left(\frac{1}{2 \ln \frac{\Lambda}{D_0}} \right) \left| \frac{\omega_P}{\omega} \right|^2 + \mathcal{O}(|\omega_P/\omega|^3). \quad (19b)$$

ω_P thus serves as a definition of the strong coupling scale, $T_P \equiv \omega_P$. The exact result in the limit $J_K = 0$ is then,

$$T_P \ln(T_P/\Lambda) = -|V| \ln \frac{\Lambda}{D_0}, \quad (20)$$

which should be contrasted with the perturbative scaling result, Eq. (14). The two definitions will be compared in Sec. (II C).

The change in thermodynamic quantities due to the introduction of such potential scattering can also be obtained from the electron Green function, Eq. (6), once the t matrix is known.⁴ At low temperatures, the behavior in the vicinity of the ALM fixed point is found to be,

$$S_{\text{imp}}(T) = -\ln(2) \left(1 + \frac{2}{\ln \frac{2T}{\Lambda}} \right) + \mathcal{O}(T^2), \quad (21a)$$

$$T\chi_{\text{imp}}(T) = \frac{1}{8} \left(1 - \frac{1}{\ln \frac{2T}{\Lambda}} \right) + \mathcal{O}(T^2). \quad (21b)$$

As confirmed by full NRG calculations below, this leading behavior arises on the lowest energy scales in the ALM phase also in the case of finite Kondo coupling, $J_K > 0$.

3. Resonant level

In the Kondo screened SSC phase of the pseudogap Kondo model, it has long been established^{13,14,27} that the lowest-energy physics is that of a simple resonant level model,

$$H_{RL} = H_0 + \tilde{v} \sum_{\mathbf{k}, \sigma} \left(c_{\mathbf{k}, \sigma}^\dagger d_\sigma + \text{H.c.} \right), \quad (22)$$

which is just the non-interacting ($U = 0$) Anderson impurity model at particle-hole symmetry. Indeed, in the present case of the defect in graphene, we show below that the lowest-energy behavior of the SSC phases can again be understood in terms of the resonant level. This motivates a brief analysis of the latter for the case where H_0 is given by Eq. (1), with corresponding local density of states, Eq. (2).

The retarded resonant level Green function is simply,

$$G_{dd}(\omega) = \frac{1}{\omega - \tilde{v}^2 G_{\text{loc}}^{(0)}(\omega) + i0^+}, \quad (23)$$

where $G_{\text{loc}}^{(0)}(\omega)$ is given in Eq. (3). The corresponding spectrum is given asymptotically by,

$$t(\omega) \stackrel{|\omega| \ll |\tilde{v}|}{\approx} \left(\frac{1}{2 \ln \frac{\Lambda}{D_0}} \right) |\omega| - \left(\frac{1}{\tilde{v}^2 \ln^2 \frac{\Lambda}{D_0}} \right) |\omega|^3 \ln \left| \frac{\omega}{\Lambda} \right| + \mathcal{O}(|\omega|^5), \quad (24a)$$

$$\stackrel{|\omega| \gg |\tilde{v}|}{\approx} \frac{1}{2} \tilde{v}^4 \ln \frac{\Lambda}{D_0} \left(\frac{1}{|\omega|^3 \ln^2 |\omega/\Lambda|} \right) + \mathcal{O}(1/|\omega|^5). \quad (24b)$$

The position of the spectral peak at ω_K is straightforwardly obtained, and the spectrum again obeys scaling as $\omega_K \rightarrow 0$ in terms of ω/ω_K ,

$$\frac{t(\omega)}{|\omega|} \Big|_{|\omega| \ll |\omega_K|} \approx \left(\frac{1}{2 \ln \frac{\Lambda}{D_0}} \right) + \left(\frac{1}{\ln \frac{\Lambda}{D_0}} \right) \left| \frac{\omega}{\omega_K} \right|^2 + \mathcal{O}(|\omega/\omega_K|^4), \quad (25a)$$

$$\Big|_{|\omega| \gg |\omega_K|} \approx \left(\frac{1}{2 \ln^2 \frac{\Lambda}{D_0}} \right) \left| \frac{\omega_K}{\omega} \right|^4 + \mathcal{O}(|\omega_K/\omega|^6), \quad (25b)$$

where $\omega_K^2 \ln |\omega_K/\Lambda| = -\tilde{v}^2 \ln(\Lambda/D_0)$.

H_{RL} should be regarded as an *effective* low-energy model here, valid in the vicinity of the SSC fixed point,^{13,14} and so the parameter \tilde{v} is itself an effective parameter. Thus, one cannot directly identify ω_K for the resonant level model with T_K for the full Kondo model with $J_K > 0$. However, the asymptotic scaling form of the spectrum, Eq. (25a), is expected to hold at low energies, as confirmed in the next section.

To lowest order, the RG scaling equations given in Eq. (13) are the same for the pure potential scatterer (with $J_K = 0$) and the Kondo model (with $V = 0$). The strong coupling scale for the former is given by Eq. (20); *mutatis mutandis*, the leading dependence of the Kondo temperature in the latter should be,

$$T_K \ln(T_K/\Lambda) = -|J_K| \ln \frac{\Lambda}{D_0}. \quad (26)$$

On the lowest energy scales in the vicinity of the SSC fixed point, thermodynamics of the full spin-1/2 Kondo model, Eq. (4), can be calculated from the effective resonant level model.^{13,14,27} The leading low-temperature behavior can again be extracted exactly from the electron Green function (or the corresponding resonant level t matrix), as shown explicitly for the entropy in Appendix B. As $T \rightarrow 0$ we find,

$$S_{\text{imp}}(T) = -\ln(4) \left(1 + \frac{1}{\ln \frac{2T}{\Lambda}} \right) + \mathcal{O}(T^2), \quad (27a)$$

$$T\chi_{\text{imp}}(T) = -\frac{1}{8} \left(1 + \frac{1}{\ln \frac{2T}{\Lambda}} \right) + \mathcal{O}(T^2). \quad (27b)$$

The low-temperature form of Eq. (27) is confirmed below by explicit NRG calculations for the full $S = 1/2$ Kondo model in the SSC phase.

B. Numerical results

The physics of the spin- S Kondo model with finite J_K and V [Eq. (4)] is obviously much more rich and subtle than the trivial limits considered above. Here, one generically expects two phases: for $J_K/|V| \gg 1$ a strong coupling (U)SSC phase should result; while an ALM phase is stable for $|V|/J_K \gg 1$. These phases are separated by a

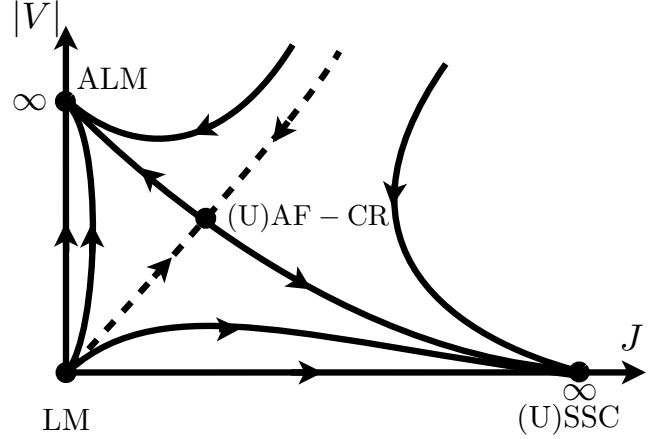


FIG. 1: Schematic phase diagram for the Kondo model with density of states given by Eq. (2) and ‘impurity’ spin $S = 1/2$ or $S = 1$. $|V|$ denotes particle-hole symmetry breaking while J_K is the Kondo coupling. Fixed points are denoted by circles, while arrowed lines refer to effective RG flow. The location of the separatrix (dashed line) depends on spin S , although the topology of the diagram is unaltered.

quantum critical point ((U)AF-CR) arising for a critical ratio $(J_K/V)_c = \mathcal{O}(1)$.

The full temperature-dependence of thermodynamic quantities can be calculated using the NRG technique.²⁴ Their characteristic behavior at the various fixed points allows straightforward identification of the phases, and the entire phase diagram can thus be mapped out. We find that the topology of the phase diagram for spin $S = 1/2$ and antiferromagnetic $J_K > 0$ is the same as for the case of the pure powerlaw density of states ($\rho(\omega) \sim |\omega|^r$ with $-1 < r < 0$) studied in Ref. 31. Indeed, the topology is unchanged for $S = 1$, although the fixed points themselves describe different physics and give rise to different thermodynamic signatures. A schematic phase diagram for the Kondo model with density of states given by Eq. (2) and spin $S = 1/2$ or $S = 1$ is presented in Fig. 1 and discussed further below.

1. $S = 1/2$ case

At high energies/temperatures, the LM fixed point describes a free and unscreened impurity local moment. The limiting high-temperature entropy is thus $S_{\text{imp}} = \ln(2)$, while the magnetic susceptibility follows the Curie law, $T\chi_{\text{imp}} = 1/4$. But the Kondo effect drives the system toward the SSC fixed point below an energy scale of order T_K when $J_K/|V| > (J_K/|V|)_c$. For $T \ll T_K$ the entropy and susceptibility for the spin-1/2 Kondo model are found from NRG to be given precisely by Eq. (27), obtained for the effective resonant level model. In particular, we note that the residual $T = 0$ entropy $S_{\text{imp}}(0) = -\ln(4)$ is the smallest possible value, because

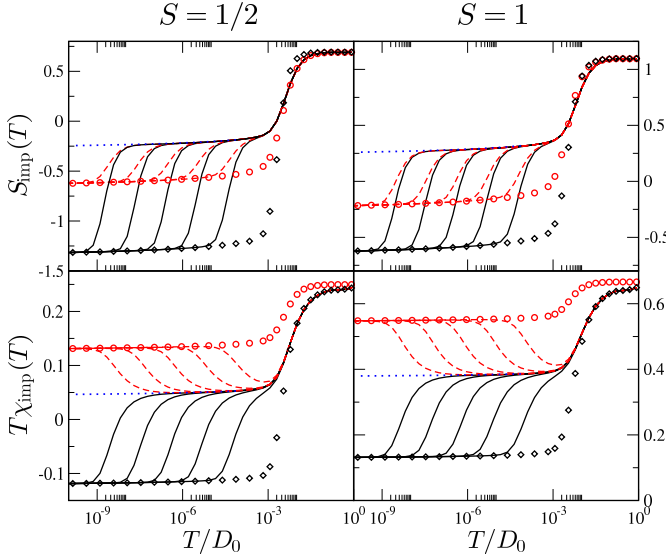


FIG. 2: Thermodynamics across the quantum phase transition for $S = 1/2$ (left panels) and $S = 1$ (right panels). Entropy $S_{\text{imp}}(T)$ (upper panels) and magnetic susceptibility $T\chi_{\text{imp}}(T)$ (lower panels) plotted vs T/D_0 for fixed $\Lambda/D_0 = 1.5$, $J_K = 0.1D_0$ and tuning $V \rightarrow V_c$. Shown for $V = V_c \pm 10^{-n}T_K^{V=0}$ with $n = 0, 1, 2, 3, 4, 5$ in order of decreasing T^* ($\propto |V - V_c|$). Solid lines for the (U)SSC phase; dashed lines for the ALM phase. The critical point itself is shown as the dotted lines. For comparison: diamond points for $J_K/D_0 = 0.1$, $V/D_0 = 0$ and circle points for $J_K/D_0 = 0$, $V/D_0 = 0.1$.

the conduction electron density of states is characterized at low energies by the strongest possible divergence (up to logarithms), while remaining normalizable.

By contrast, for $J_K/|V| < (J_K/|V|)_c$ the ALM fixed point is stable, and describes maximal particle-hole asymmetry. The crossover from LM to ALM physics occurs on the strong coupling scale, T_P . The free impurity local moment is then supplemented by an anomalous host contribution to give $T \rightarrow 0$ thermodynamics described by Eq. (27). The precise agreement on the lowest energy scales confirms the physical interpretation of the fixed point in terms of the pure potential scatterer discussed above.

On fine-tuning in the vicinity of the critical point $J_K/|V| \simeq (J_K/|V|)_c$, RG flow from the high-energy LM fixed point to the stable fixed point describing the ground state occurs via the critical point, AF-CR. Two universal scales can thus be identified in this regime: T_c ($\approx T_K$) sets the scale for onset of criticality associated with AF-CR, while T^* ($\propto |V - V_c|$) characterizes the ultimate crossover to either SSC or ALM fixed points (depending on the sign of $V - V_c$). The distinctive asymptotic thermodynamic properties of each fixed point are summarized in Table I.

Remarkably, the impurity entropy at ALM, AF-CR, and SSC fixed points is negative. We note, however, that all thermodynamic quantities flow to their respective

TABLE I: Properties of fixed points for $S = 1/2$

	$\lim_{T \rightarrow 0} S_{\text{imp}}$	$\lim_{T \rightarrow 0} T\chi_{\text{imp}}$
ALM	$-\ln 2$	$1/8$
LM	$\ln 2$	$1/4$
AF-CR	$-\ln 4/3$	$1/24$
SSC	$-\ln 4$	$-1/8$

zero-temperature values logarithmically slowly. This is a direct consequence of the logarithmic energy dependence in the density of states, see Eq. (2)

The left panels of Fig. 2 show the full crossovers in the entropy and susceptibility calculated numerically exactly using NRG. In both cases, diamond points show the direct crossover from LM to SSC arising for $J_K/D_0 = 0.1$ but $V/D_0 = 0$; while circle points show the direct crossover from LM to ALM when $V/D_0 = 0.1$ but $J_K/D_0 = 0$. Thermodynamics are also shown on tuning to the quantum critical point (dotted line). Approach from the SSC phase (solid lines) and the ALM phase (dashed lines) exhibit two characteristic scales, T_c and T^* , as above.

Dynamical quantities, such as the $T = 0$ scattering t matrix, similarly evince the rich RG structure of the problem. In Fig. 3 (upper panel) we plot the scaling spectra $t(\omega)/|\omega|$ vs $|\omega/\omega_K|$ for a system deep in the SSC phase (solid and dotted lines). Its asymptotic behavior at both high and low energies is found to be described by Eq. (25).

In the ALM phase (Fig. 3, center panel), the scaling spectrum $t(\omega)/|\omega|$ vs $|\omega/\omega_P|$ is asymptotically described by Eq. (19). In particular, we note the more gentle linear approach to the Fermi level, and the inherent asymmetry of the spectrum, arising due to the relevance of particle-hole symmetry-breaking.

The lower panel of Fig. 3 shows a critical spectrum, plotted as $t(\omega)/|\omega|$ vs $|\omega/\omega_c|$. The resonance around $\omega = \text{sgn}[\omega V]|\omega_c|$ is split, with the peaks separated by $\sim |V - J_K|$. At low energies $|\omega| \ll |\omega_c|$ the spectrum $t(\omega)/|\omega| \sim a + b \text{sgn}[\omega V]|\omega/\omega_c|$ has a leading linear dependence.

2. $S = 1$ case

In the case of a spin-1 Kondo ‘impurity’ (obtained at low-energies from Eq. (1) when $G = \frac{J_H}{4U_{\sigma\pi}} \gg 1$), the phase diagram is topologically equivalent to that of the spin $S = 1/2$ case (see Fig. 1). The thermodynamic properties of the fixed points themselves are summarized in Table II.

TABLE II: Properties of fixed points for $S = 1$

	$\lim_{T \rightarrow 0} S_{\text{imp}}$	$\lim_{T \rightarrow 0} T\chi_{\text{imp}}$
ALM	$-\ln 4/3$	$13/24$
LM	$\ln 3$	$2/3$
UAF-CR	$\ln 5/4$	$3/8$
USSC	$-\ln 2$	$1/8$

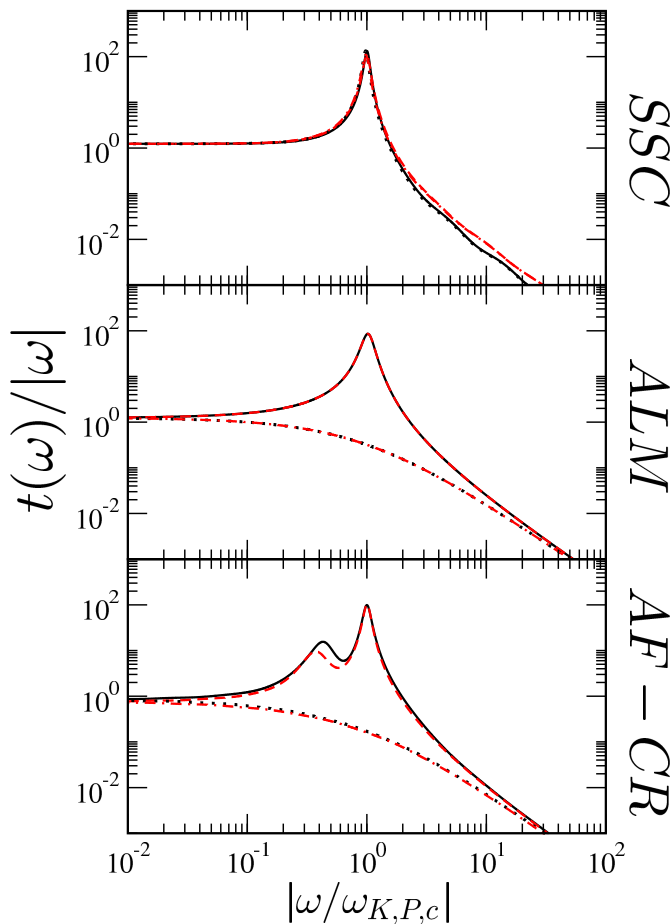


FIG. 3: Spectral function $t(\omega)/|\omega|$ at $T = 0$. For impurity spin $S = 1/2$: $\omega > 0$ and $\omega < 0$ plotted as solid and dotted lines. For impurity spin $S = 1$: $\omega > 0$ and $\omega < 0$ plotted as dashed and dot-dashed lines. Top panel: vs $|\omega/\omega_K|$ in the SSC phase ($J_K = 10^{-6}D_0$ and $V/J_K = 0$ and 0.01). Middle panel: vs $|\omega/\omega_P|$ in the ALM phase ($V = 10^{-6}D_0$ and $J_K/V = 0$ and 0.01). Lower panel: vs $|\omega/\omega_c|$ at the critical point ($J_K = 10^{-6}D_0$ and $V/J_K = (V/J_K)_c$). $\Lambda/D_0 = 1.5$ used throughout. Asymptotes discussed in the text.

The LM fixed point again describes the high-energy/temperature behavior of the $S = 1$ Kondo model. However, the free impurity moment is now a spin-1 object, which gives rise to $S_{\text{imp}} = \ln(3)$ and $T\chi_{\text{imp}} = \frac{2}{3}$, as seen clearly for all data in the right-hand panels of Fig. 2.

For $J_K/|V| < (J_K/|V|)_c$, relevant particle-hole symmetry breaking drives the system to the ALM fixed point below T_P . The free spin-1 impurity moment is then supplemented by the anomalous host contribution to give $S_{\text{imp}} = \ln(3) - \ln(4)$ and $T\chi_{\text{imp}} = \frac{2}{3} - \frac{1}{8}$. The direct crossover from LM to ALM is shown as the circle points in the right-hand panels of Fig. 2.

For $J_K/|V| > (J_K/|V|)_c$, the Kondo effect drives the system to the USSC fixed point below T_K . For spin-1, the impurity is however *underscreened*: the conduction electrons only partially compensate the impurity moment. Asymptotically, a free impurity spin-1/2 moment

remains. Together with the anomalous host contribution, one then obtains $S_{\text{imp}} = \ln(2) - \ln(4)$ and $T\chi_{\text{imp}} = \frac{1}{4} - \frac{1}{8}$. The direct crossover from LM to USSC is shown as the diamond points in the right-hand panels of Fig. 2.

In the vicinity of the quantum critical point, $J_K/|V| \simeq (J_K/|V|)_c$, two scales again emerge. Flow toward the unstable UAF-CR critical point on the scale of T_c ($\sim T_K$) is followed ultimately by flow to the ALM or USSC fixed points below T^* ($\sim |V - V_c|$), which describe the $T = 0$ ground state of either phase. The right-hand panels of Fig. 2 also show the full temperature-dependence of the impurity contribution to the entropy, $S_{\text{imp}}(T)$ (upper panel), and magnetic susceptibility, $T\chi_{\text{imp}}(T)$ (lower panel), as the critical point (dotted line) is approached from the USSC phase (solid lines) and the ALM phase (dashed lines). As with the spin-1/2 case, the approach to all fixed points occurs logarithmically slowly as a direct consequence of the explicit logarithmic energy dependence of the density of states, Eq. (2).

Scaling spectra $t(\omega)/|\omega|$ at $T = 0$ for systems in the USSC phase (upper panel, vs $|\omega/\omega_K|$), ALM phase (middle panel, vs $|\omega/\omega_P|$) and at the UAF-CR critical point (lower panel, vs $|\omega/\omega_c|$) are shown in Fig. 3 as the dashed and dotted lines. They are characterized by the same asymptotic behavior as the spin-1/2 case, described by Eqs. (19) and (25).

C. Evolution of T_K and T_P

Solution of the generalized poor man's scaling equations for the spin $S = 1/2$ and $S = 1$ models gives an estimate for the strong coupling scales T_K and T_P , Eq. (14). In the trivial potential scattering limit considered explicitly in Sec. II A 2, the scale T_P can be obtained exactly, Eq. (20). Up to logarithms, one thus expects in either case the same linear dependence of the strong coupling scale $T_P \sim V$ or $T_K \sim J_K$.

Here we calculate T_P and T_K numerically exactly using NRG³⁴ for a wide range of systems with $S = 1/2$ and $S = 1$, varying V , J_K and the cutoff Λ . In Fig. 4 we plot $T_K \ln(\Lambda/T_K)/\ln(\Lambda/D_0)$ vs J_K/D_0 for systems in the (U)SSC phase, and $T_P \ln(\Lambda/T_P)/\ln(\Lambda/D_0)$ vs V/D_0 for systems in the ALM phase. The excellent agreement, especially for small J_K or V , confirms Eqs. (26) and (20) (solid line). For comparison, the result of Eq. (14) is shown as the dashed line.

III. ANDERSON MODEL

We consider now the full Andersonian model for the graphene vacancy, Eq. (1).

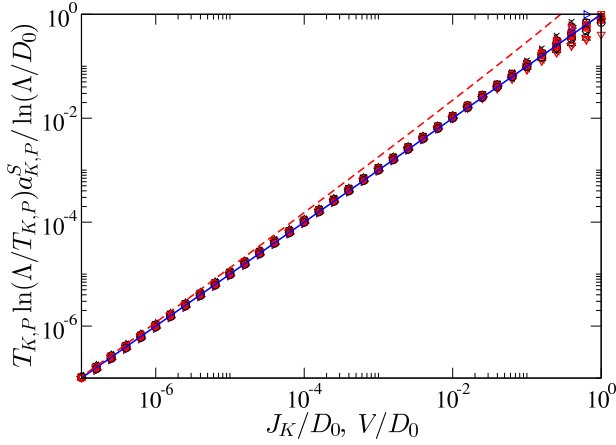


FIG. 4: T_K and T_P extracted from NRG calculations for various values of J_K and V deep in the SSC phase ($J_K/V = 2$) and the ALM phase ($J_K/V = 1/2$) for both $S = 1/2$ and $S = 1$ and $\Lambda/D_0 = 100, 10, 1.1, 1.01, 1.001$. All data plotted as $T_{K,P} \ln(\Lambda/T_{K,P}) a_{K,P}^S / \ln(\Lambda/D_0)$ vs J_K/D_0 or V/D_0 [the constant $a_{K,P}^S = \mathcal{O}(1)$ depends only on the phase (SSC or ALM) and on the impurity spin S]. Data collapse to the analytic result [Eq. (20), solid line], is found at small J_K, V . For comparison, Eq. (14) for $\Lambda = 10$ is shown as the dashed line.

A. Accessibility of the ALM phases

In Sec. II we discussed the rich phase diagram of the Kondo models with $S = 1/2$ and $S = 1$. In both cases, these models were derived from an Andersonian model (which also allows for charge fluctuations), by projecting onto the ‘impurity’ spin-manifold using a Schrieffer-Wolff transformation. Within this leading-order perturbative treatment, Eq. (5) indicates that the maximum ratio of the effective potential scattering, V , and the effective Kondo exchange coupling, J_K is given by

$$\left| \frac{V}{J_K} \right| \leq \frac{1}{4}. \quad (28)$$

The natural question is then: which of the strong coupling phases of a Kondo model can actually be accessed within the bare Anderson model. In order to answer this, we study the exact position of the phase boundary of the effective $S = 1/2$ and $S = 1$ Kondo models; and examine directly the full Andersonian model, Eq. (1).

Fig. 5 shows the phase diagram of the Kondo models for both spin $S = 1/2$ (diamond points) and $S = 1$ (circle points), obtained numerically exactly using NRG. The inset shows the asymptotic small- J_K behavior, which is found to follow

$$\left| \frac{V}{J_K} \right|_c = a_S + b \ln(J_K/\Lambda), \quad (29)$$

with $a_{S=1/2} = 3/4$, $a_{S=1} = 1$ and $b \approx -0.3$ for $\Lambda/D_0 = 1.5$ (see dashed lines).

For comparison, we also plot the Schrieffer-Wolff result, Eq. (28), as the dotted line in Fig. 5. The obvious

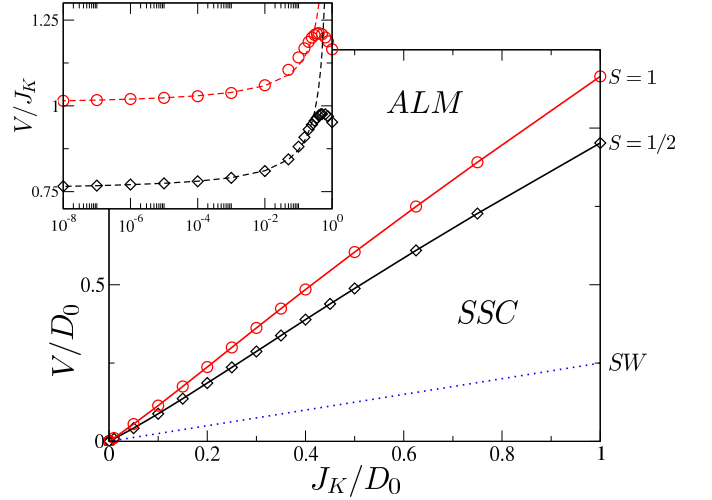


FIG. 5: Phase diagram in the $J_K - V$ plane for $\Lambda/D_0 = 1.5$, indicating the critical separatrix between (U)SSC and ALM phases for impurity spin $S = 1/2$ and $S = 1$. At small J_K , the critical ratio $|V/J_K|_c$ is given by Eq. (29) [see inset, dashed lines]. The regime of validity of the effective Kondo model is given by the Schrieffer-Wolff asymptote $|V/J_K|_{\max} = 1/4$, shown as the dotted line.

conclusion is that the effective potential scattering, V , derived from the bare Andersonian model is never large enough to access the ALM phase. A numerical survey of the parameter space of Eq. (1) supports this result, and suggests that the Kondo effect is always operative at the lowest energy scales. The ground state is thus described by the SSC (or USSC) fixed point.

We note, however, that this conclusion strictly applies only to the model with simplified density of states given in Eq. (2). Very strong particle-hole asymmetry in the density of states at high energies could in principle change this picture.

B. The doublet-triplet transition

Tuning the Hund’s coupling, J_H , in Eq. (1) allows to access either $S = 1/2$ or $S = 1$ sectors of the isolated ‘impurity’ manifold. On coupling to the conduction electrons for finite v_{hyb} , effective low-energy Kondo models can then be derived with definite impurity spin, which have different stable fixed points (SSC for $S = 1/2$ but USSC for $S = 1$). Since the two ground states cannot be continuously connected (they have, for example, different residual entropy), one expects a quantum phase transition on tuning J_H in the full model, which we call DT-CR.

This scenario is explored in Fig. 6, where we take representative model parameters for the Andersonian model, and fine-tune J_H across the transition. Solid lines correspond to the SSC doublet phase [$J_H < (J_H)_c$], while dashed lines are for systems in the USSC triplet phase [$J_H > (J_H)_c$]. The critical point itself is shown as the

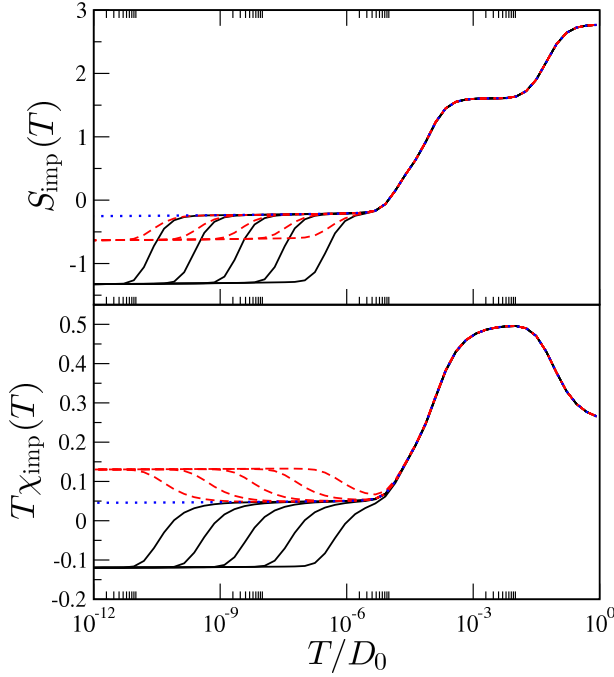


FIG. 6: Thermodynamics $S_{\text{imp}}(T)$ and $T\chi_{\text{imp}}(T)$ vs T/D_0 across the quantum phase transition, separating doublet and triplet phases of the full model, Eq. (1), on tuning the Hund's coupling J_H . Parameters are $\Lambda/D_0 = 1.5$, $U/D_0 = 0.3$, $\epsilon/D_0 = -0.15$, $U_{\sigma\pi}/D_0 = 0.025$, $v_{\text{hyb}}/D_0 = 0.008$, $g/D_0 = 0.008$, varying $J_H/D_0 = (J_H)_c \pm 10^{-n} T_K^{J_H=0}$ with $n = 0, 1, 2, 3, 4$ approaching progressively the critical point at $(J_H)_c \simeq 0.101 D_0$ (dotted line). For $J_H < (J_H)_c$ the doublet phase is obtained (solid lines); while $J_H > (J_H)_c$ yields the triplet phase (dashed lines). The transition is characteristic of a level-crossing.

TABLE III: Properties of fixed points for the full model

	$\lim_{T \rightarrow 0} S_{\text{imp}}$	$\lim_{T \rightarrow 0} T\chi_{\text{imp}}$
SSC	$-\ln 4$	$-1/8$
USSC	$-\ln 2$	$1/8$
DT-CR	$-\ln 4/3$	$1/24$

dotted line. The asymptotic thermodynamic properties of the fixed points are also given in Table III.

We find that the doublet-triplet transition is characteristic of a level-crossing: the low-energy scale setting the crossover from DT-CR to either SSC or USSC has the linear dependence $T^* \sim |J_H - (J_H)_c|$. Physical properties at the point of transition can be understood simply in terms of coexisting SSC and USSC fixed points.

Deep in either doublet SSC or triplet USSC phase, we have confirmed by direct numerical calculation that the low-energy physics is that of the corresponding $S = 1/2$ or $S = 1$ Kondo models in the SSC or USSC phases.

IV. CONCLUSIONS

In this paper we studied the physics of a reconstructed vacancy in an otherwise perfect graphene sheet. The defect is modelled in terms of a generalized Anderson model with a diverging density of states following a recent paper by Cazalilla *et al.*¹⁹ We combined analytical and numerical techniques to obtain a rather complete understanding of the model and its properties.

When charge fluctuations are frozen out, the complex orbital structure of the Andersonian model can be more simply understood in terms of an effective spin-1/2 or spin-1 object exchange-coupled to the graphene host. These doublet and triplet Kondo models are unusual due to the modified graphene conduction electron density of states, which results in a strongly enhanced *linear* scaling of the Kondo temperature with coupling strength, $T_K \sim J_K$ (up to logarithms) and anomalous ground state thermodynamic properties. For example, in the doublet phase, the residual impurity contribution to the entropy assumes the minimum possible value for a quantum impurity problem of this type, $S_{\text{imp}}(T \rightarrow 0) = -k_B \ln(4)$. Furthermore, it leads to a rich phase diagram, because particle-hole symmetry-breaking is relevant. Unlike the situation in standard metals, a new stable strong coupling phase is supported in these Kondo models, characterized by large renormalized potential scattering, which suppresses the Kondo effect. A more conventional strong coupling phase is also supported, associated with a large renormalized Kondo coupling (although anomalous host contributions to certain physical quantities are again shown to appear). The two phases are separated by an unstable quantum critical point. We supplement our detailed numerical study with analytic treatment of simple effective models which describe the physics in the vicinity of the two strong coupling fixed points.

However, direct analysis of the full Andersonian model reveals that the phase transition separating the two strong coupling phases cannot in practice be accessed, because the effective Kondo coupling and effective potential scattering are slaved. In consequence, the Kondo effect is *always* operative on the lowest energy scales in the graphene system with isolated vacancies, modelled by Eq. (1). In principle, potential scattering from other sources could manifest at higher energies ($|\omega| > \Lambda$, not considered here). If sufficiently strong, we note that the particle-hole asymmetric local moment phase could be stabilized; although the distortion of the density of states required for this makes it unlikely.

The existence of *two* effective Kondo models with distinct spin implies the presence of a quantum phase transition in the full Andersonian model between exactly-screened spin-1/2 Kondo and underscreened spin-1 Kondo phases. We demonstrated that this transition can be realized on tuning the Hund's coupling, and find that the transition is characteristic of a first-order level crossing. We study both phases and the transition between them using the NRG technique.

As expected from the Schrieffer-Wolff mapping, the low-energy physics of the full model for the isolated graphene vacancy is indeed shown to be described by effective Kondo models in their Kondo screened phases. The unusual physics of the generalized Kondo problem with strongly divergent conduction density of states is thus expected in such systems.

Acknowledgements

We acknowledge useful discussions with Ralf Bulla, Matthias Vojta and Martin Galpin. This work was supported by the DFG under FR 2627/3-1 (LF), SFB 608 (AKM,LF) and FOR 960 (AKM); and by the EPSRC through EP/1032487/1 (AKM).

Appendix A: Local Green function

The derivation of the local Green function at low frequencies is straightforward but tedious. In the following we sketch it: while the imaginary part follows trivially from the density of states the real part has to be evaluated from Kramers-Kronig relation

$$G_{\text{loc}}^{(0)}(\omega) = \mathcal{P} \int d\epsilon \frac{\rho(\epsilon)}{\omega - \epsilon} - i\pi\rho(\omega). \quad (\text{A1})$$

The real part can be brought into the form

$$\Re G_{\text{loc}}^{(0)}(\omega) = \ln \frac{\Lambda}{D_0} \frac{\text{sgn}(\omega)}{|\omega|} \mathcal{P} \int_0^{\frac{D_0}{|\omega|}} \frac{dE}{(1-E^2)E \ln^2 \frac{E|\omega|}{\Lambda}}. \quad (\text{A2})$$

After an integration by parts one arrives at

$$\begin{aligned} \frac{\text{sgn}(\omega)|\omega|}{\ln \frac{\Lambda}{D_0}} \Re G_{\text{loc}}^{(0)}(\omega) &= \lim_{\delta \rightarrow 0} \left[-\frac{1}{\ln \frac{E|\omega|}{\Lambda}(1-E^2)} \right]_0^{1-\delta} \\ &+ \lim_{\delta \rightarrow 0} \left[-\frac{1}{\ln \frac{E|\omega|}{\Lambda}(1-E^2)} \right]_{1+\delta}^{\frac{D_0}{|\omega|}} \\ &+ \lim_{\delta \rightarrow 0} \int_0^{1-\delta} \frac{2EdE}{(1-E^2)^2 \ln \frac{E|\omega|}{\Lambda}} \\ &+ \lim_{\delta \rightarrow 0} \int_{1+\delta}^{\frac{D_0}{|\omega|}} \frac{2EdE}{(1-E^2)^2 \ln \frac{E|\omega|}{\Lambda}}. \end{aligned} \quad (\text{A3})$$

At this point it is important to notice that in the limit $|\omega| \ll \Lambda$ we can rewrite the above expression to leading

order

$$\begin{aligned} \frac{\text{sgn}(\omega)|\omega|}{\ln \frac{\Lambda}{D_0}} \Re G_{\text{loc}}^{(0)}(\omega) &\approx \lim_{\delta \rightarrow 0} \left[-\frac{1}{\ln \frac{E|\omega|}{\Lambda}(1-E^2)} \right]_0^{1-\delta} \\ &+ \lim_{\delta \rightarrow 0} \left[-\frac{1}{\ln \frac{E|\omega|}{\Lambda}(1-E^2)} \right]_{1+\delta}^{\frac{D_0}{|\omega|}} \\ &+ \lim_{\delta \rightarrow 0} \frac{1}{\ln \frac{|\omega|}{\Lambda}} \int_0^{1-\delta} \frac{2EdE}{(1-E^2)^2} \\ &+ \lim_{\delta \rightarrow 0} \frac{1}{\ln \frac{|\omega|}{\Lambda}} \int_{1+\delta}^{\frac{D_0}{|\omega|}} \frac{2EdE}{(1-E^2)^2}. \end{aligned} \quad (\text{A4})$$

This expression directly leads to Eq. (3).

Appendix B: Logarithmic corrections

Here we obtain analytically the first logarithmic correction to the impurity entropy, from the free energy of an effective resonant level model. The general formula to calculate the free energy of a local level is given by

$$\mathcal{F} = -T \sum_{\sigma} \sum_{\omega_n} \ln(-G_{\sigma}^{-1}(\omega_n)) e^{i\omega_n 0^+} \quad (\text{B1})$$

Using residual calculus this can be converted into a line integral along the branch cut along the real axis given by

$$\mathcal{F} = - \sum_{\sigma} \int_{-\infty}^{\infty} \frac{dz}{\pi} n_F(z) e^{z0^+} \text{Im} \ln(-G_{r,\sigma}^{-1}(z)) \quad (\text{B2})$$

where the subscript r refers to the retarded Green function. Consequently, we obtain the entropy as

$$S = -\frac{\partial \mathcal{F}}{\partial T} = \int_{-\infty}^{\infty} \frac{dz}{\pi} \frac{2}{\cosh^2 z} \text{Im} \ln(-G_{r,\sigma}^{-1}(z2T)) , \quad (\text{B3})$$

where the factor of two is due to the spin summation. The low-energy properties will be entirely dominated by the self-energy, which is of the form

$$\Sigma(z) \approx \tilde{v}^2 \frac{\pi \ln \frac{\Lambda}{D_0}}{2|z| \ln^2 \left| \frac{z}{\Lambda} \right|} \left(\ln \left| \frac{z}{\Lambda} \right| \frac{2}{\pi} \text{sgn}(z) + i \right). \quad (\text{B4})$$

It is then straightforward to derive an expression for the impurity entropy. It follows as,

$$S = - \int_0^{\infty} \frac{dz}{\pi} \frac{2z}{\cosh^2 z} \left(\pi + 2 \arctan \frac{\pi}{2 \ln \left| \frac{2Tz}{\Lambda} \right|} \right) \quad (\text{B5})$$

Realizing the low-temperature limit, this can be approximated as,

$$S \approx - \int_0^{\infty} dz \frac{2z}{\cosh^2 z} \left(1 + \frac{1}{\ln \left| \frac{2Tz}{\Lambda} \right|} \right) \quad (\text{B6})$$

which, to leading order, yields

$$S \approx -\ln 4 \left(1 + \frac{1}{\ln \left| \frac{2T}{\Lambda} \right|} \right). \quad (\text{B7})$$

-
- ¹ K. S. Novoselov, A. K. Geim, S. V. Morozov, D. Jiang, Y. Zhang, S. V. Dubonos, I. V. Grigorieva, and A. A. Firsov, *Science* **306**, 666 (2004).
- ² K. S. Novoselov, A. K. Geim, S. V. Morozov, D. Jiang, M. I. Katsnelson, I. V. Grigorieva, S. V. Dubonos, and A. A. Firsov, *Nature* **438**, 197 (2005).
- ³ A. H. Castro Neto, F. Guinea, N. M. R. Peres, K. S. Novoselov, and A. K. Geim, *Rev. Mod. Phys.* **81**, 109 (2009).
- ⁴ A. C. Hewson, *The Kondo Problem to Heavy Fermions* (Cambridge University Press, Cambridge, 1993).
- ⁵ H. B. Zhuang, Q.-F. Sun, and X. C. Xie, *Europhys. Lett.* **86**, 58004 (2009).
- ⁶ P. S. Cornaglia, G. Usaj, and C. A. Balseiro, *Phys. Rev. Lett.* **102**, 046801 (2009).
- ⁷ B. Uchoa, V. N. Kotov, N. M. R. Peres, and A. H. Castro Neto, *Phys. Rev. Lett.* **101**, 026805 (2008).
- ⁸ B. Uchoa, L. Yang, S.-W. Tsai, N. M. R. Peres, and A. H. Castro Neto, *Phys. Rev. Lett.* **103**, 206804 (2009).
- ⁹ Z.-G. Zhu, K.-H. Ding, and J. Berakdar, *Europhys. Lett.* **90**, 67001 (2010).
- ¹⁰ M. Vojta, L. Fritz, and R. Bulla, *Europhys. Lett.* **90**, 27006 (2010).
- ¹¹ D. Withoff and E. Fradkin, *Phys. Rev. Lett.* **64**, 1835 (1990).
- ¹² C. Gonzalez-Buxton and K. Ingersent, *Phys. Rev. B* **57**, 14254 (1998).
- ¹³ M. Vojta and L. Fritz, *Phys. Rev. B* **70**, 094502 (2004).
- ¹⁴ L. Fritz and M. Vojta, *Phys. Rev. B* **70**, 214427 (2004).
- ¹⁵ J. O. Sofo, G. Usaj, P. S. Cornaglia, A. M. Suarez, A. D. Hernandez-Nieves, and C. A. Balseiro, *Phys. Rev. B* **85**, 115405 (2012).
- ¹⁶ J. J. Palacios, and F. Yndurain, *preprint arXiv:1203.6485* (2012).
- ¹⁷ P. Haase, S. Fuchs, T. Pruschke, H. Ochoa, and F. Guinea, *Phys. Rev. B* **83**, 241408(R) (2011).
- ¹⁸ T. Kanao, H. Matsuura, and M. Ogata, *J. Phys. Soc. Jpn.* **81**, 063709 (2012).
- ¹⁹ M. A. Cazalilla, A. Iucci, F. Guinea, and A. H. Castro Neto, *preprint arXiv:1207.3135* (2012).
- ²⁰ R. R. Nair, M. Sepioni, I.-L. Tsai, O. Lehtinen, J. Keinonen, A. V. Krashenninnikov, T. Thomson, A. K. Geim, and I. V. Grigorieva, *Nat. Phys.* **8**, 199 (2012).
- ²¹ K. M. McCreary, A. G. Swartz, W. Han, J. Fabian, and R. K. Kawakami, *preprint arXiv:1206.2628* (2012).
- ²² J.-H. Chen, L. Li, W. G. Cullen, E. D. Williams, and M. S. Fuhrer, *Nat. Phys.* **7**, 535 (2011).
- ²³ L. Fritz and M. Vojta, *preprint arXiv:1208.3113* (2012).
- ²⁴ R. Bulla, T. Costi, and T. Pruschke, *Rev. Mod. Phys.* **80**, 395 (2008).
- ²⁵ Following Ref. 19, we assume throughout that $\epsilon_\pi \simeq 0$, $-U < \epsilon_d < 0$, and $U_{\sigma\pi}$, $J_H > 0$. The tunnel-couplings are also taken to be small, $v_{\text{hyb}}^2, g^2 \ll U$.
- ²⁶ C. R. Cassanello and E. Fradkin, *Phys. Rev. B* **53**, 15079 (1996).
- ²⁷ M. T. Glossop and D. E. Logan, *Eur. Phys. J. B* **13**, 513 (2000).
- ²⁸ D. E. Logan and M. T. Glossop, *J. Phys.: Condens. Matter* **12**, 985 (2000).
- ²⁹ R. Bulla, M. T. Glossop, D. E. Logan, and T. Pruschke, *J. Phys.: Condens. Matter* **12**, 4899 (2000).
- ³⁰ M. Vojta, *Phil. Mag.* **86**, 1807 (2006).
- ³¹ M. Vojta and R. Bulla, *Eur. Phys. J. B* **82**, 283 (2002).
- ³² A. K. Mitchell, L. Fritz, R. Bulla, and M. Vojta, *to appear*.
- ³³ P. W. Anderson, *J. Phys. C* **3**, 2436 (1970).
- ³⁴ The values of T_K and T_P are determined in practice from NRG as the point where the impurity contribution to the entropy is halfway between the high-temperature LM fixed point and low-temperature (U)SSC or ALM fixed point values: $S_{\text{imp}}(T_{K,P}) = \frac{1}{2}[S_{\text{imp}}(\infty) - S_{\text{imp}}(0)]$.